

Impulse load characteristics of bouldery debris flow impact

D. SONG*†, C. E. CHOI‡§, G. G. D. ZHOU‡§, J. S. H. KWAN|| and H. Y. SZE||

Boulders entrained in debris flows are the main cause of damage to debris-resisting structures. Poly-dispersity leads to grain-size segregation, which causes boulders to migrate to the free surface and then accumulate at the front of the flow. Despite the importance of grain-size segregation, the current design of debris-resisting structures does not explicitly consider its effects on impact. In this study, two series of centrifuge tests were carried out to investigate the impact behaviour of mono-disperse bouldery flows and bi-disperse flows comprising boulders mixed with fine debris material. The diameter of the boulders was varied to study the effects of boulder size on the dynamic response of an instrumented model rigid barrier. The results reveal that, as the boulder size increases, a transition from progressive loading to predominantly impulse loading is observed. Boulders floating on the fine debris can induce even higher peak loads compared with mono-disperse bouldery flow. A new relationship between an equivalent dynamic pressure coefficient for the hydrodynamic approach and boulder size is established. This new relationship serves as a criterion for distinguishing between the boulders and fine debris in the design of structural countermeasures.

KEYWORDS: centrifuge modelling; landslides; particle-scale behaviour

ICE Publishing: all rights reserved

NOTATION

E	Young's modulus (GPa)
E_B	elastic modulus of barrier (Pa)
E_b	elastic modulus of boulder (Pa)
F_b	impact load of single boulder
F_d	impact load of the fine debris
g	gravitational acceleration
h	flow depth (m)
K_c	load reduction factor
l	flow length
m_b	radius of boulder (kg)
N	scale factor
p	impact pressure
r_b	radius of boulder (m)
v	flow velocity (m/s)
v_b	velocity of boulder (m/s)
w	debris width (m)
α	dynamic pressure coefficient
δ	boulder diameter
μ	Poisson's ratio
μ_B	Poisson's ratio of barrier
μ_b	Poisson's ratio of boulder
ρ	debris bulk density (kg/m^3)

INTRODUCTION

Boulders (or hard inclusions) in debris flows are primarily responsible for the incapacitation of protection structures

(Zeng *et al.*, 2015), owing to their destructive impulse loads. According to the findings of field monitoring, impact force of debris flows is 'saw-tooth' like as a result of the fluid movement with multiple-sized boulders (Zhang, 1993). The random boulder-impact loading is far greater than the long-term fine debris pressures (Hu *et al.*, 2011). However, the current design of debris-resisting structures relies on empiricism and only considers the impulse load from a single boulder (Hung *et al.*, 1984; Kwan, 2012).

The design debris flow impact force is taken as the superposition of fine debris impact load and boulder impact load. For the impact of fine debris, the impact load F_d is calculated based on the conservation of momentum (hydrodynamic approach, Hung *et al.*, 1984; Hübl *et al.*, 2009)

$$F_d = \alpha \rho v^2 h w \quad (1)$$

where α is dynamic pressure coefficient (2.5 from Kwan, 2012; 1.5 from Hung *et al.*, 1984) to account for discrepancies attributed to the simplifications and assumptions between theoretical predictions and physical measurements (Song *et al.*, 2017), ρ the debris bulk density (kg/m^3), v the flow velocity (m/s), h the flow depth (m) and w the debris width (m). For single boulder impact, the impact load F_b is calculated based on the Hertz contact theory (Hung *et al.*, 1984; VanDine, 1996; SWCB, 2005; Kwan, 2012)

$$F_b = K_c n a^{1.5} \quad (2)$$

$$n = \frac{4r_b^{0.5}}{3\pi(k_b + k_B)} \quad (3)$$

$$a = \left[\frac{5m_b v_b^{2.7}}{4n} \right]^{0.4} \quad (4)$$

$$k_b = \frac{1 - \mu_b^2}{\pi E_b} \quad (5)$$

$$k_B = \frac{1 - \mu_B^2}{\pi E_B} \quad (6)$$

Manuscript received 19 November 2017; first decision 10 April 2018; accepted 10 April 2018.

Published online at www.geotechniqueletters.com on 19 June 2018.

*Key Laboratory of Mountain Hazards and Earth Surface Process/Institute of Mountain Hazards and Environment, Chinese Academy of Sciences (CAS), Chengdu, China.

†University of Chinese Academy of Sciences, Beijing, China.

‡Department of Civil and Environmental Engineering, Hong Kong University of Science and Technology, Clear Water Bay, Kowloon, Hong Kong.

§The HKUST Jockey Club Institute for Advanced Study, Hong Kong.

||Geotechnical Engineering Office, Civil Engineering and Development Department, Hong Kong SAR.

where, K_c is the load reduction factor (0.1 for rigid barrier with consideration of plastic deformation of concrete (Hungr *et al.*, 1984; Kwan, 2012)), r_b the radius of the boulder (m), m_b the radius of the boulder (kg), v_b the velocity of the boulder (m/s), E_b the elastic modulus of the boulder (Pa), μ_b is Poisson's ratio of the boulder and E_B the elastic modulus of the barrier (Pa), μ_B is Poisson's ratio of the barrier, respectively.

Evidently, interactions between boulders and fine debris in equations (1) and (2) are not explicitly considered. More specifically, grain-size segregation (Johnson *et al.*, 2012; Cui *et al.*, 2017a) and cushioning effects of fine debris during impact, are neglected. In order to consider the effects of grain-size segregation it is necessary to characterise the loading behaviour of a wide range of particle sizes. However, there lacks a scientific criterion to clearly distinguish the particle sizes, which are capable of generating sharp impulse loads and the particle sizes that can be treated as part of the fine debris.

Finally, another scientific challenge of studying debris flows is that they are stress-dependent phenomena (Cui *et al.*, 2017b). Small-scale models cannot capture the correct stress-dependent response of a granular assembly. Therefore, centrifuge modelling is a suitable approach to ensure that the prototype stress states can be reasonably approximated by elevating the centrifugal gravitational field in a model (Bowman *et al.*, 2010; Ng *et al.*, 2016a). This study takes advantage of centrifuge modelling to investigate mono-disperse boulder flows impacting a rigid barrier. The loading characteristics are then compared with that of bi-disperse boulder-sand mixtures to reveal the effects of fine debris.

CENTRIFUGE MODELLING OF BOULDERY FLOW IMPACT

Scaling

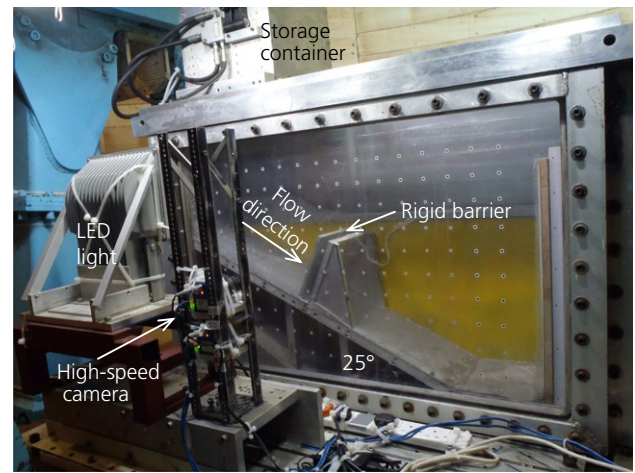
The downslope motion of debris flows is driven by gravitational potential. More specifically, the flow inertia can be characterised using a velocity scale $v = (gl)^{1/2}$ (Iverson *et al.*, 2004), where g is the gravitational acceleration and l the flow length. In centrifuge modelling, the gravitational acceleration increases N times and linear dimensions (e.g. l and boulder diameter δ) reduce N times, resulting in a scale factor of unity for velocity. Based on the conservation of momentum, the debris impact pressure ($p \sim \rho v^2$) on the barrier is the same as that in prototype. The debris impact force ($F_b \sim \rho v^2 h w$) on the barrier has a scale factor of $1/N^2$ (Ng *et al.*, 2016a). It is the same with the debris impact, the boulder impact force corresponds with the Hertz equation and has a scale factor of $1/N^2$. The details for scaling laws are discussed in Ng *et al.* (2016a) and Chu & Zhang (2010) and relevant scaling laws are summarised in Table 1.

Model set-up and instrumentation

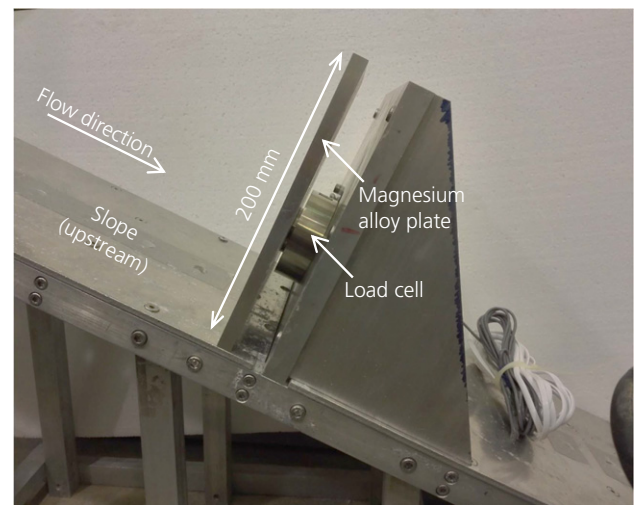
Figure 1(a) shows a side view of the model package on the centrifuge platform at the Hong Kong University of Science and Technology. The 400 g-t centrifuge has an arm radius of

Table 1. Relevant scaling laws (Schofield, 1980; Ng *et al.*, 2016a)

Parameter	Dimension	Scaling law (model/prototype)
Gravity	L/T^2	$N = 22.4$
Density	M/L^3	1
Length (l and diameter δ)	L	$1/N$
Velocity	L/T	1
Inertial time	T	$1/N$
Pressure	$M/(T^2L)$	1
Force	ML/T^2	$1/N^2$



(a)



(b)

Fig. 1. (a) Side view of model set-up on centrifuge platform; (b) set-up and instrumentation of rigid barrier (all dimensions model scale). Load cell is positioned at lower 1/3 of the barrier height

4.2 m (Ng, 2014). The model container is 1245 mm long, 350 mm wide and 850 mm deep. The container has a Perspex window for capturing the kinematics of each test. Inside the model container, the Perspex of the container and a partition are used to form a channelised slope, 233 mm wide and 1000 mm long. The slope is inclined at 25° and supported by an aluminium frame. A storage container with a volume of 0.03 m³ is installed above the slope at the upstream end of the channel. The storage container has a hinged door at the bottom, which is controlled using a hydraulic actuator. The opening of this hinged door releases debris in-flight on to the channel.

A magnesium alloy plate, 200 mm high and 233 mm wide, was installed perpendicularly to the slope to model a rigid barrier. A single through-hole compression load cell was adopted to measure the total load induced on the barrier (Fig. 1(b)). The interaction time is scaled down to $1/N$ of the prototype (Table 1); therefore, a sampling rate of 20 kHz was selected to ensure that details of the dynamic process are captured. A high-speed camera was used to capture the kinematics during each test. The high-speed camera frame rate was set to 640 fps at a resolution of 1300 × 1600 pixels.

Boulders and debris materials

Uniform glass spheres with diameters of 3, 10, 22 and 39 mm were used to model boulders of various sizes.

Under an elevated gravitational acceleration condition (22.4g), the glass spheres are equivalent to prototype boulders of diameter of 70, 220, 490 and 870 mm, respectively (Fig. 2). Leighton Buzzard fraction C sand comprising fairly uniform and rounded grains with diameter of about 0.6 mm was used to model the fine debris of the bi-disperse flows.

The glass spheres have Young's modulus similar to that of granitic rock. While the modulus of the magnesium alloy plate is similar to the upper limit of that of reinforced concrete (Table 2). The friction angle of each granular material was measured using tilting tests and is 30–31°. The glass spheres experienced less frictional resistance than angular particles, hence the measured impact forces are on the conservative side.

Test procedure and test programme

Prior to conducting impact tests, a series of calibration tests without a rigid barrier were carried out to characterise the typical flow depth and frontal velocity using a high-speed camera (Table 3). In the calibration, flow depth is defined as the steady depth after the tapered flow front passes through



Fig. 2. Boulder and debris materials: glass spheres and Leighton Buzzard fraction C sand

Table 2. Properties of glass spheres and rigid barrier

Material	Young's modulus, E : GPa	Poisson's ratio, μ	Friction angle: °*
Boulder (granite)	30–60	0.20–0.30	45–60
Reinforced concrete	26–38	0.30	50–60
Glass sphere	60	0.25	30–31
Magnesium alloy	40	0.30	31
Sand	0.001	0.20–0.25	31

*Interface friction angle is determined by friction angles of the contact pair, whichever is lower.

Table 3. Test programme of bouldery debris impact (all dimensions in model scale)

Test ID	Material	Prototype boulder diameter, δ : mm	Bulk density: kg/m^3	Frontal velocity: m/s	Prototype flow depth, h : mm	Normalised boulder diameter, δ/h
B3	Glass spheres (3 mm)	70	1539	14.2 ± 0.2	1030 ± 35	0.07
B10	Glass spheres (10 mm)	220	1611	21.9 ± 0.8	1187 ± 110	0.19
B22	Glass spheres (22 mm)	490	1583	9.4 ± 1.8	1344 ± 245	0.37
B39	Glass spheres (39 mm)	870	1513	9.1	870	1.00
B10S	Glass spheres (10 mm) + LB fraction C sand	220	1822	11.4 ± 0.8	585 ± 110	0.38
B22S	Glass spheres (22 mm) + LB fraction C sand	490	1831	9.1 ± 1.8	663 ± 245	0.74
B39S	Glass spheres (39 mm) + LB fraction C sand	870	1822	8.7	870	1.00

the location where a rigid barrier would be installed. With the known distance and the difference in time of the approaching flow front, the average frontal velocity can be deduced. Errors of measurement mainly originate from the determination of frontal velocity and flow depth that are high-speed image based. Except the 39 mm glass sphere tests (RB39 and RB39S), which are characterised with flow depth of only one time of particle diameter, determination of the flow front and free flow surface may have an error rate of about half of the particle diameter. The frontal velocity and flow depth are summarised in Table 3 and error bars are shown in Fig. 6.

To study the influence of particle dispersity on the dynamic barrier response, mono-disperse (glass spheres) and bi-disperse (glass spheres–sand mixture) flows were adopted to impact the barrier. The bi-disperse flows comprise 30% glass spheres in volume. Due to the formation of dead zone (Ng *et al.*, 2016a) in the impact process, boulders entrained at the tail of flow would not have chance to directly impact the barrier. Thus when preparing the debris in storage containers, the boulders concentrated at the bottom half of the debris. Specifically, the boulders formed the skeleton of the sample and sand was then rained to fill the void of the boulders. Accordingly, the bulk density in Table 3 refers to the front half of the flow. The 15 litre bouldery debris in this study is equivalent to a prototype volume of 170 m^3 . The impact test programme is summarised in Table 3.

RESULTS AND INTERPRETATION

Impact kinematics

Typical impact kinematics for bi-disperse flows comprising boulders 870 mm in diameter in prototype (test B39S) is shown in Fig. 3. As the bi-disperse flow reaches the base of the rigid barrier, the formation of a dead zone is observed ($t = 1.6 \text{ s}$, Fig. 3(a)). Afterwards, the processes of kinetic sieving and induced grain-size segregation (Wang & Hutter, 2001; Hill & Fan, 2008; Zhou & Ng, 2010) are evident ($t = 1.9 \text{ s}$, Fig. 3(b)). The fine debris (sand) falls through the large voids formed by large glass spheres to the bottom of the flow, whereas, the boulders tend to shift to the free surface and migrate to the front of the flow. As a result of grain-size segregation, the approaching velocity of the boulders is not attenuated simultaneously with the dry sand. The maximum velocity is observed near the free surface where the glass spheres float on the sand. The effects of the formation of a dead zone and the process of grain-size segregation have significant effects on the impact force and will be discussed in the following section.

Influence of mono-dispersity: glass spheres impact

Figure 4 shows the effects of increasing boulder diameter on the dynamic response of the rigid barrier. For mono-disperse

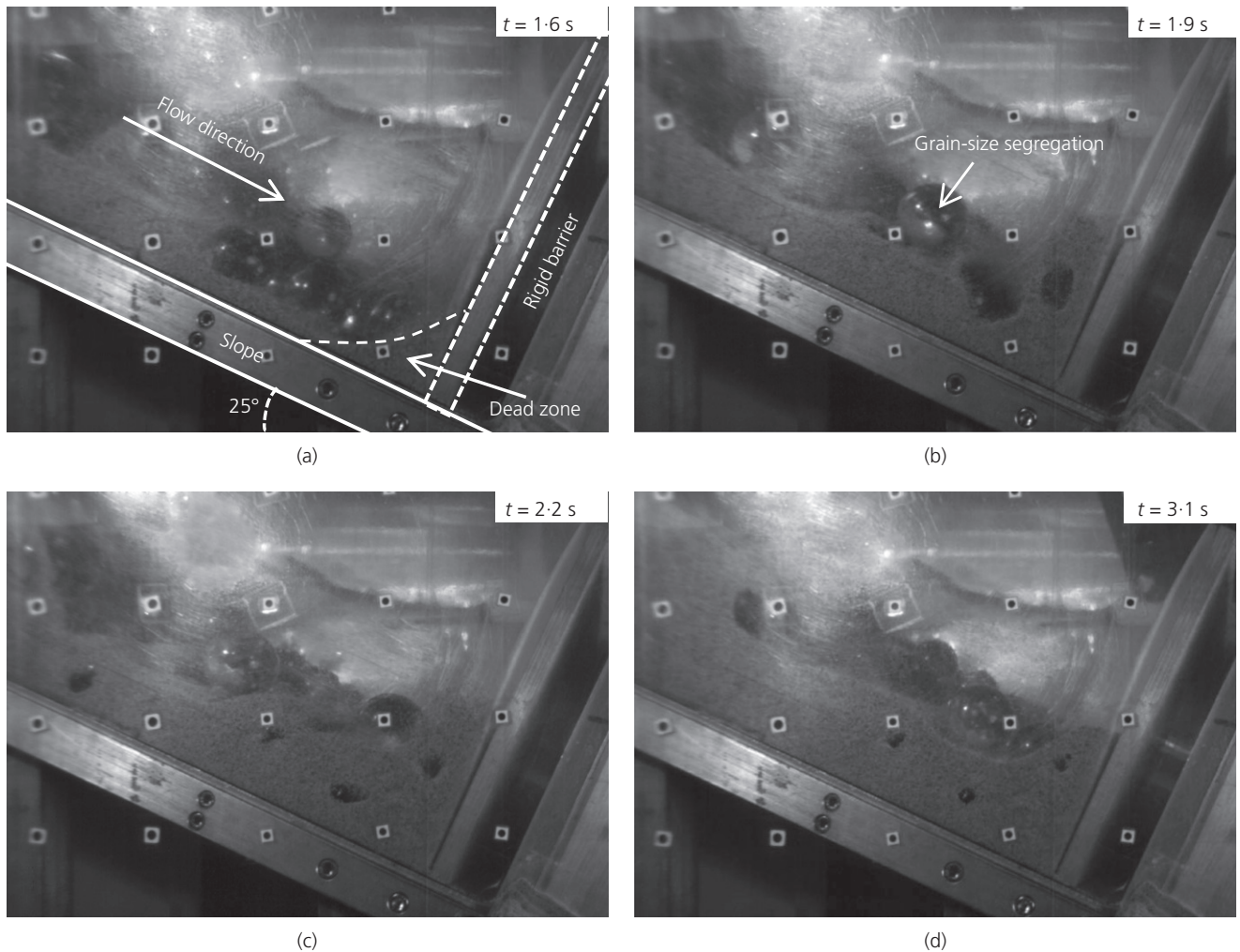


Fig. 3. Observed interaction kinematics for test B39S in prototype time (a) $t = 1.6$ s; (b) $t = 1.9$ s; (c) $t = 2.2$ s and (d) $t = 3.1$ s. The initial interaction times are reset to 1.0 s (0.045 s) as the flow front impacts the barrier

flows comprising boulders that are 70 mm in prototype (test B3), the force–time history shows relatively small fluctuations and the maximum impact force is the static load near the end of the impact process (Fig. 4(a)). With an increase of the boulder size, loading transitions from the characteristic of continuum impact to that of discrete impact on the rigid barrier (Fig. 4(b)). Impulse loads are more dominant for discrete loading and apparent for mono-disperse flows with larger boulder with diameters of 490 mm in prototype (test B22, Fig. 4(c)). A multitude of sharp impulses from individual spheres are observed. For the test where the largest mono-disperse spheres was used (870 mm in prototype, test B39), peak impulses induced by the boulders are highly transient with duration of 0.015 s in prototype. The measured peak impulse is as high as 2900 kN, which is about 6 times the static load (Fig. 4(d)).

Influence of bi-dispersity: glass spheres–sand mixture impact

Figure 5 shows impact time histories for bi-disperse flows comprising glass spheres of varying diameters and dry sand within the matrix of the flow. Comparison between the effects of mono- and bi-dispersity reveals that the bi-disperse flows with fine debris within the matrix exhibit remarkably less impulses compared with the mono-disperse glass spheres. The bi-disperse flows mixed with prototype diameter of 220 mm (B10S, Fig. 5(a)) show considerably less

impulse and relatively smoother progressive loading than the other tests (B10, Fig. 4(b)). This indicates that the sand is effective at cushioning the glass spheres during the impact process.

Less impulse is also observed in 870 mm diameter test with fine debris (Figs 4(d) and 5(c)). However, the dynamic response of the bi-disperse flow (test B39S) shows even higher peak load than the mono-disperse counterpart (test B39). The peak impact loads of bi-disperse flows comprise two loading components, more specifically, the static load formed from the dead zone of fine debris (Fig. 3(a)) and the dynamic impulse load from the discrete glass sphere impacts. Nonetheless, in both cases (tests B39 and B39S), the dynamic components are both about 2900 kN. Evidently, the process of grain-size segregation, which exhibits floating glass spheres at the free surface and accumulate at the flow front, allows the large glass spheres to travel relatively unimpeded with limited velocity reduction. The boulders floating on the fine debris have similar velocity with sand, thus there is little relative movement and the energy dissipation is limited.

As discussed above, the cushioning effect of fine debris results in less impulses compared to the mono-disperse flows. Also, the static load of fine debris causes the total peak load of bi-disperse flow higher than that of mono-disperse flow. These denote the major differences between tests RB39 and RB39S. On the other hand, they do share some similarity. Owing to the effect of grain-size segregation, the

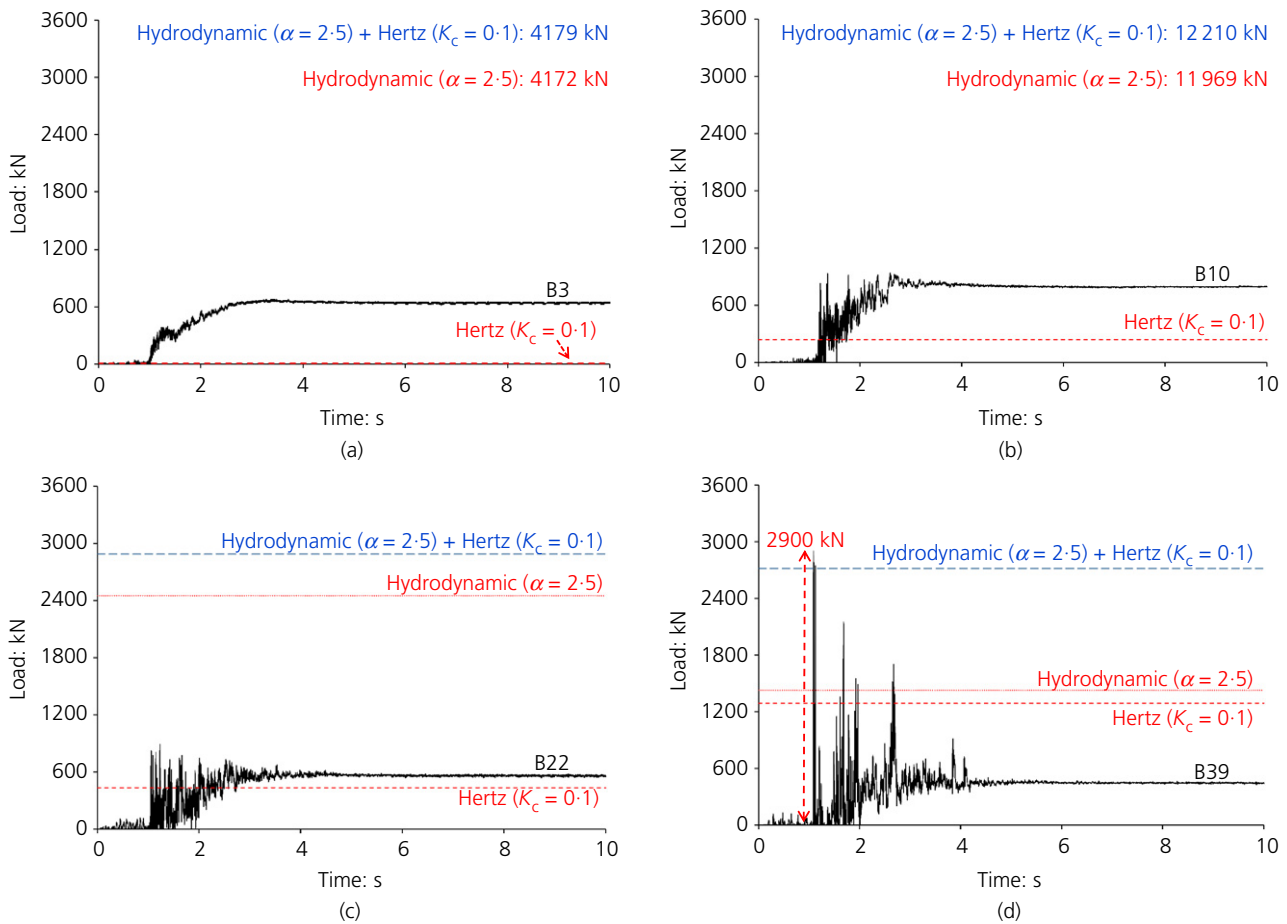


Fig. 4. Comparison of impact forces induced by boulders (a) B3; (b) B10; (c) B22; and (d) B39

'floating' boulders impact the rigid barrier without the cushioning effect of dry sand, resulting in similarly high-impulse loads (2900 kN, Figs 4(d) and 5(c)) for both mono- and bi-disperse flows. If the static load is not considered, the 'floating' boulders of bi-disperse flow is equivalent to the flow front of a mono-disperse flow. Considering the close frontal velocities in tests RB39 (9.1 m/s) and RB39S (8.7 m/s, Table 3), the consistent dynamic impulse components, to some extent, confirm the repeatability of the tests.

The impact loads in Figs 4 and 5 are also compared with the design forces according to the guidelines (with $\alpha = 2.5$ and $K_c = 0.1$, Kwan, 2012). For the bouldery debris impact on a rigid barrier, the total impact load is the superposition of both fine debris and boulder impact loads. Therefore, three reference lines are plotted on each figure. As the boulder diameter δ is much smaller than the flow depth h – that is $\delta/h = 0.07$ for the 70 mm glass spheres impact (test B3), the impulse load of single particle predicted by equation (2) is negligible (Fig. 4(a)). However, for the flow with a diameter of 870 mm (test B39, Fig. 4(d)), the single boulder impact load is even larger than the debris impact (equation (1)). The combination of the fine debris and single boulder impact loads can generally bind the measured loads, except for the bi-disperse 870 mm flow mixed with sand (test B39S) where the grain-size segregation results in 21% higher load (Fig. 5(c)) than the mono-disperse flow (Fig. 4(d)).

Effects of boulder size and design criterion

This study aims to ascertain a criterion under which boulder diameter can be bounded using a particular dynamic

pressure coefficient α from the hydrodynamic approach (equation (1)). In terms of contribution of boulder impact to the total impact load, the definition of boulder should be a relative concept and vary with the scale of debris flows. Instead of the absolute particle diameter, the normalised boulder diameter, ratio between boulder diameter and flow depth δ/h , is adopted for the quantitative comparison. Figure 6 shows the relationship between the back-calculated α and the normalised particle diameter δ/h . Since α is deduced directly from the peak force, loads due to both the fine debris and boulders are implicitly considered.

The results show that α is insensitive to the small boulder diameter with δ/h from 0.07 to 0.19 (70–220 mm, prototype diameters). However, α increases almost linearly as the diameter of the boulder increases from 0.19 to 1.00 (220–870 mm). The mono-disperse flows correspond higher α than the bi-disperse flows, which is conservative for a design purpose. For instance, using an $\alpha = 2.5$ (Kwan, 2012) for equation (1), impulses are covered for a 1.0 m deep flow with 0.6 m diameter boulders impacting a rigid barrier. This indicates that for those normalised boulder diameter larger than 0.6, single boulder impact should be considered separately using Hertz equation (equation (2)). Similarly, $\alpha = 1.5$ recommended by Hungr *et al.* (1984) could cover boulders with diameter 0.45 times the flow depth (Fig. 6). The relationship between the back-calculated α and the normalised particle diameter provides quantitative criteria for distinguishing boulders, which could induce sharp impulse and the particles that could be treated as fine debris. However, only limited data points are available at the current stage. More physical data are needed to verify the relationship between the back-calculated α and the

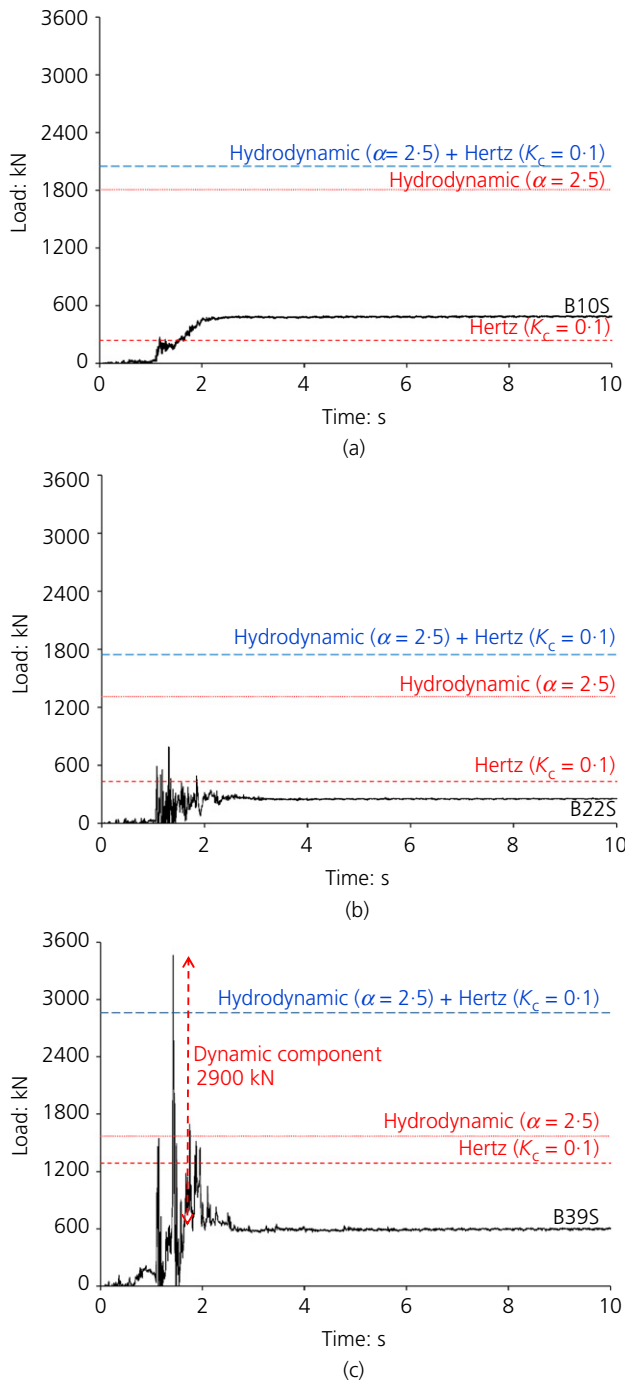


Fig. 5. Comparison of impact forces induced by boulder-debris mixtures (a) B10S; (b) B22S; and (c) B39S

normalised particle diameter, especially the range of normalised particle diameter 0.4–1.0.

Owing to the inertial effects of massive protection structures, short-duration boulder impact usually contributes to localised structural failure (Yang *et al.*, 2012; Zeng *et al.*, 2015). Except for sizeable boulder impulse impact, fine debris impact is likely the main concern for global geotechnical instability. In this case, adopting an exceptionally high α value (e.g. $\alpha > 2.5$) to cover the boulder impact load as part of the debris impact load may yield over-conservative design rendering it non-economical. Rather, adding a cushioning layer in the front of rigid walls suffice to attenuate the impulse loads. Specifically, a 1 m thick gabion cushioning layer could effectively reduce the K_c to 0.05 for repeated boulder impacts (Ng *et al.*, 2016b).

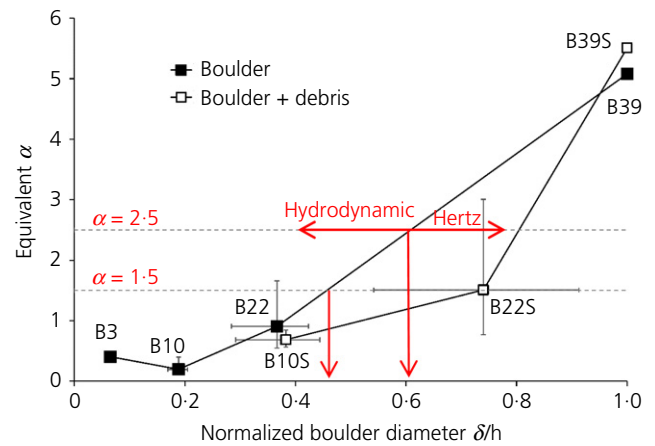


Fig. 6. Relationship between particle size and dynamic pressure coefficient α

CONCLUSIONS

An interpretation of the results pertaining to mono- and bi-disperse flows impacting a rigid barrier is presented in this study. The mono-disperse flows resemble bouldery flows, whereas the bi-disperse flows resemble larger boulders with fine debris within its matrix. The results reveal that discrete impulse loading is strongly influenced by the boulder diameter. With the increase of boulder size, the transient impulse loading by individual boulder dominates the rigid barrier response. The fine debris within the matrix can also provide a cushioning effect, which is manifested in the dynamic response of the barrier with more attenuated impulses. However, the effects of grain-size segregation of bi-disperse flows enable the migration of larger particles to the free surface, which are relatively unimpeded and result in peak loads exceeding those observed from mono-disperse flows. By studying a wide range of particle sizes in this study, results show that the hydrodynamic equation, using an $\alpha = 2.5$, can bound impulses from boulders of up to 0.6 times of the flow depth for rigid barrier impact. The relationship between the back-calculated α and the normalised particle diameter in Fig. 6 forms a basis for distinguishing between fine debris and sizable boulders, which induce sharp impulses for the impact of debris flows.

ACKNOWLEDGEMENTS

The authors are grateful for the financial support from the theme-based research grant T22-603/15N and the general research fund 16209717 provided by the Research Grants Council of the Government of Hong Kong SAR, China. The authors are also grateful for the financial sponsorship from the Chinese Academy of Sciences (CAS) Pioneer Hundred Talents Program and National Natural Science Foundation of China (11672318; 51709052). They are also grateful for the support by the HKUST Jockey Club Institute for Advanced Study and the financial support by the Hong Kong Jockey Club Disaster Preparedness and Response Institute (HKJCDPRI18EG01). This paper is published with the permission of the head of the Geotechnical Engineering Office and the director of Civil Engineering and Development, the Government of the Hong Kong Special Administrative Region.

REFERENCES

- Bowman, E. T., Laue, J., Imre, B. & Springman, S. M. (2010). Experimental modelling of debris flow behaviour using a geotechnical centrifuge. *Can. Geotech. J.* **47**, No. 7, 742–762.

- Chu, L. M. & Zhang, L. M. (2010). Centrifuge modeling of ship impact loads on bridge pile foundations. *J. Geotech. Geoenviron. Engng* **137**, No. 4, 405–420.
- Cui, Y. F., Zhou, X. J. & Guo, C. X. (2017a). Experimental study on the moving characteristics of fine grains in wide grading unconsolidated soil under heavy rainfall. *J. Mt. Sci.* **14**, No. 43, 417–431.
- Cui, Y. F., Chan, D. & Nouri, A. (2017b). Discontinuum modeling of solid deformation pore-water diffusion coupling. *Int. J. Geomech.* **17**, No. 8, 04017033, [https://doi.org/10.1061/\(ASCE\)GM.1943-5622.0000903](https://doi.org/10.1061/(ASCE)GM.1943-5622.0000903).
- Hill, K. M. & Fan, Y. (2008). Isolating segregation mechanisms in a split-bottom cell. *Phys. Rev. Lett.* **101**, No. 8, 088001.
- Hu, K., Wei, F. & Li, Y. (2011). Real-time measurement and preliminary analysis of debris-flow impact force at Jiangjia Ravine, China. *Earth Surf. Process. Landf.* **36**, No. 9, 1268–1278.
- Hübl, J., Suda, J., Proske, D., Kaitna, R. & Scheidl, C. (2009). Debris flow impact estimation. In *Proceedings of the 11th international symposium on water management and hydraulic engineering*, Ohrid, Macedonia (ed. C. Popovska), pp. 1–5. Skopje, Macedonia: University of Ss Cyril and Methodius, Faculty of Civil Engineering.
- Hungr, O., Morgan, G. C. & Kellerhals, R. (1984). Quantitative analysis of debris torrent hazards for design of remedial measures. *Can. Geotech. J.* **21**, No. 4, 663–677.
- Iverson, R. M., Logan, M. & Denlinger, R. P. (2004). Granular avalanches across irregular three-dimensional terrain: 2. Experimental tests. *J. Geophys. Res.: Earth Surf.* **109**, No. F1, F01015, <https://doi.org/10.1029/2003JF000084>.
- Johnson, C. G., Kokelaar, B. P., Iverson, R. M., Logan, M., LaHusen, R. G. & Gray, J. M. N. T. (2012). Grain-size segregation and levee formation in geophysical mass flows. *J. Geophys. Res.* **117**, No. F1, F01032, <https://doi.org/10.1029/2011JF002185>.
- Kwan, J. S. H. (2012). *Supplementary technical guidance on design of rigid debris-resisting barriers*, GEO Report number 270. Hong Kong SAR: Geotechnical Engineering Office.
- Ng, C. W. W. (2014). The state-of-the-art centrifuge modelling of geotechnical problems at HKUST. *J. Zhejiang Univ. Sci. A* **15**, No. 1, 1–21.
- Ng, C. W. W., Song, D., Choi, C. E., Koo, R. C. H. & Kwan, J. S. H. (2016a). A novel flexible barrier for landslide impact in centrifuge. *Geotech. Lett.* **6**, No. 3, 221–225, <https://doi.org/10.1680/jgele.16.00048>.
- Ng, C. W. W., Choi, C. E., Su, A. Y., Kwan, J. S. H. & Lam, C. (2016b). Large-scale successive boulder impacts on a rigid barrier shielded by gabions. *Can. Geotech. J.* **53**, No. 10, 1688–1699.
- Schofield, A. N. (1980). Cambridge geotechnical centrifuge operations. *Géotechnique* **30**, No. 3, 227–268, <https://doi.org/10.1680/geot.1980.30.3.227>.
- Song, D., Choi, C. E., Ng, C. W. W. & Zhou, G. G. D. (2017). Geophysical flows impacting a flexible barrier: effects of solid-fluid interaction. *Landslides* **15**, No. 1, 99–110.
- SWCB (2005). *Manual of soil and water conservation*. Taiwan, Republic of China: Soil and Water Conservation Bureau (in Chinese).
- VanDine, D. F. (1996). *Debris flow control structures for forest engineering*. Victoria, BC, Canada: Ministry of Forests.
- Wang, Y. & Hutter, K. (2001). Granular material theories revisited. In *Geomorphological Fluid Mechanics. Lecture Notes in Physics* (eds N. J. Balmforth and A. Provenzale), vol. 582, pp. 79–107. Berlin, Heidelberg, Germany: Springer.
- Yang, Y., Lam, N. T. K. & Zhang, L. (2012). Evaluation of simplified methods of estimating beam responses to impact. *Int. J. Struct. Stab. Dynam.* **12**, No. 3, 1250016.
- Zeng, C., Cui, P., Su, Z., Lei, Y. & Chen, R. (2015). Failure modes of reinforced concrete columns of buildings under debris flow impact. *Landslides* **12**, No. 3, 561–571.
- Zhang, S. (1993). A comprehensive approach to the observation and prevention of debris flows in China. *Nat. Hazards*, **7**, No. 1, 1–23.
- Zhou, G. G. D. & Ng, C. W. W. (2010). Dimensional analysis of natural debris flows. *Can. Geotech. J.* **47**, No. 7, 719–729.

HOW CAN YOU CONTRIBUTE?

To discuss this paper, please submit up to 500 words to the editor at journals@ice.org.uk. Your contribution will be forwarded to the author(s) for a reply and, if considered appropriate by the editorial board, it will be published as a discussion in a future issue of the journal.